Eur. Phys. J. D **42**, 217–220 (2007)
DOI: 10.1140/epjd/e2007-00021-1

THE EUROPEAN PHYSICAL JOURNAL D

Isotopomer selective optimization of $^{39}K^{85}Rb^+$ and $^{41}K^{87}Rb^+$ using optimal control

A. Merli[a], F. Sauer, L. Wöste, and A. Lindinger

Institut für Experimentalphysik, Freie Universität Berlin, Arnimallee 14, 14195 Berlin, Germany

Received 8 June 2006 / Received in final form 17 November 2006
Published online 31 January 2007 –

Abstract. We report on isotope selective three-photon ionization of two isotopomers of KRb by applying evolution strategies. The particularity of this experiment is based on the high resolution phase and amplitude modulation of the fs-laser pulses provided by a 2×640 pixel pulse shaper. The optimization in a closed feedback loop performed with spectrally broad pulses centered at 840 nm shows high enhancements of one isotopomer at the expense of the other isotopomer and vice versa. From the optimal laser field we aim to gain details about the selective ionization sequence and the wavepacket evolution on the involved vibrational states.

PACS. 82.53.-k Femtochemistry – 28.60.+s Isotope separation and enrichment – 33.80.Rv Multiphoton ionization and excitation to highly excited states (e.g., Rydberg states)

1 Introduction

The high interest in experiments with cold and ultracold heteronuclear alkali mixtures was stimulating to further investigate them and their isotopomers. In order to receive information about the selectivity of different isotopomers a feedback control experiment on the ionization processes of alkali dimers was applied. The approach of adaptive femtosecond quantum control follows the suggestion of Judson and Rabitz [1], in which a computer-controlled pulse shaper is used in combination with a self-learning algorithm [2] and direct feedback from the experiment to achieve coherent control over photoinduced processes. This occurs in an automated fashion, without requiring any model for the systems response. The aim of most optimization experiments was to achieve maximal yields for selective objectives [3–7]. One exciting aspect of the adaptive feedback control was to decipher the reaction mechanism by encoding the acquired optimal pulse shape [8–10]. Theoretical support in the conceptualization of the principles of coherent control, as well as providing designs for the control fields to manipulate molecules and interpretation of the resulted optimal pulse form was given by several groups [11–15].

Recently, we reported isotope selective ionization by optimal control on the K_2 and NaK system [16,17]. From the optimal pulse shapes we extracted information about the dynamics on the involved vibrational states. The feasibility of the method for the $^{39}K^{85}Rb^+$/ $^{41}K^{87}Rb^+$ isotopomer ratio by first applying a high resolution pulse shaper for closed feedback loop experiments is demonstrated in this paper. Potassium has two naturally occurring isotopes (^{39}K, 93.26% and ^{41}K, 6.73%) and rubidium also has two isotopes (^{85}Rb, 72.17% and ^{87}Rb, 27.83%). The relative abundance of the four KRb isotopomeres is given by: $^{39}K^{85}Rb$ 67.3%, $^{41}K^{85}Rb$ 4.9%, $^{39}K^{87}Rb$ 26.0%, and $^{41}K^{87}Rb$ 1.9%. The isotopomers $^{39}K^{85}Rb$ and $^{41}K^{87}Rb$ were selected for this particular optimized isotope-selective ionization experiment due to the highest mass difference.

The electronic states of KRb have been theoretically investigated by Leininger and Jeung [18] and by Park et al. [19] who applied a method based on restricted Hartree-Fock calculations. Their model is based on a small-core relativistic pseudopotential taking nine valence electrons for each atom into consideration [20] using configuration interaction. Spectroscopical studies on KRb and their isotopomers in a pulsed molecular beam were performed by resonance enhanced two photon ionization (RE2PI) at 530 nm by Lee et al. [21]. They showed new electric quadrupole transitions $1\ ^1\Delta \longleftarrow X(1)^1\Sigma^+$ of KRb. The same group observed hyperfine splitting of the $^{39}K^{85}Rb$ and $^{39}K^{87}Rb$ lines in mass-resolved RE2PI studies [22]. These results indicate that high resolution pulse shaping technique can be helpful for exploring the potential energy levels of the KRb system without exact previous knowledge of these and for finding the relevant transitions for the optimal isotopomer selectivity process.

[a] e-mail: merli@physik.fu-berlin.de

2 Experimental set-up

The KRb dimers are produced by coexpansion of potassium and rubidium vapor with argon as carrier gas through a nozzle with 80 μm diameter into the vacuum. The oven with the alkali mixture was heated to about 300 °C and the carrier gas pressure was set to 2 bars. After passing a skimmer, the cluster beam enters the detection chamber which has a pressure of 10^{-7} mbar. As a result a ro-vibrationally cold molecular beam was produced. The multiphoton ionization of KRb was achieved by interrogating the cluster beam with the focused fs-laser light between the ion optic elements of the quadrupole mass spectrometer (QMS). The outcoming photoions were mass-selected with a resolution $m/\Delta m$ higher than 200. The arising ion current was measured by a secondary electron multiplier (SEM). In addition to KRb and its isotopomers, the recorded mass spectra shows peaks of K, K_2, Rb and Rb_2 as well. The ion signals of both isotopomers are acquired alternatively on two different channels of the QMS and digitized by an analog-to-digital converter (SR 245). The beam fluctuation was 2% for the lighter and about 10% for the heavier isotopomer.

A Ti:sapphire oscillator (Mira; Coherent) pumped by a Nd:YVO_4 cw-laser (Verdi V5; Coherent) provides fs-pulses of low energy, so the experiment was performed in the weak field regime, which simplified the interpretation of the resulting pulse forms. The oscillator generates laser pulses with a repetition rate of 76 MHz, a spectral width of $\Delta\lambda \approx 30$ nm, and an energy of 6.8 nJ per pulse. The central wavelength for this particular experiment was set to $\lambda = 840$ nm.

A pulse shaper was used to modify the spectral components of the pulses, which allowed simultaneous and independent phase- and amplitude-modulation [23]. The liquid crystal spatial light modulator (SLM-640; CRI) consisting of 2×640 pixels was placed in the Fourier plane of a double grating zero dispersion compressor [24]. The high pixel number in combination with 2000 lines/mm gratings and lenses with a focal length of $f = 250$ mm provide a spectral resolution of 0.127 nm/pixel for this experiment. A similar pulse shaper built by Monmayrant et al. [25–27] was used for quantum state measurements using coherent transients.

Our implemented closed loop experiment couples the ion detection with the programmable pulse shaper that is driven by a self-learning optimization algorithm based on evolution strategies. An initial population of 10 random individuals (10 pulse forms) is created corresponding to 10 different patterns of the 640 phase and/or 640 amplitude values of the laser field. After recombination and mutation 30 offspring are provided and written on the modulator mask. The ion signal determines the quality of each individual. The 10 best individuals are selected and serve as parents for the next generation. Details about the optimization algorithm can be found in [28]. The generated optimized pulse form is characterized by the acquired pulse spectra and by frequency resolved cross correlation (XFROG), where the cross correlation traces of the shaped test pulse and the reference short pulse are recorded for different frequencies.

3 Results and discussion

The goal of the evolution algorithm was to find the optimal laser field (at 840 nm center wavelength) which maximizes or minimizes the fitness ratio defined as $R = {}^{39}K^{85}Rb^+/{}^{41}K^{87}Rb^+$. By simultaneous phase and amplitude modulation, the algorithm enhanced the isotopomer ratio to $R_{max} = 145$ after approximately 155 generations. This value is about a factor of 4 larger than the ratio obtained by an unshaped transform limited pulse ($R_n = 35.4$). During the minimization, the algorithm decreased the ratio to $R_{min} = 8$, which is by a factor of 4.4 smaller than R_n. In total, but not simultaneously, the phase and amplitude modulated laser pulse amounts to an optimization factor of about $R_{tot} = 18$ between maximization and minimization. Also pure amplitude and pure phase optimization for maximization and minimization of the isotopomer ratio was performed. The achieved total factors of $R_{tot} = 2.4$ for amplitude only and $R_{tot} = 1.8$ for phase only measurements confirm that simultaneous phase and amplitude optimization is more selective.

In order to extract information about the underlying isotope selection process the spectra of the phase and amplitude modulated optimized pulses which gave the best ratios for the maximization and minimization were analyzed. Figure 1 shows numerous sharp peaks with different intensities for both pulses. Due to the high shaper resolution and the large bandwidth of the laser pulse, multiple vibronic transitions predominantly from the electronic ground state $X(1)^1\Sigma^+$; $v'' = 0$ to the first excited $A(2)^1\Sigma^+$ state of the KRb dimer can be identified. About 10 vibrational levels are excited in the $A(2)^1\Sigma^+$ state and the pronounced ones are indicated in Figure 1 for the maximization (a) and for the minimization (b), respectively. Some vibronic transitions observed in the maximization experiment were not present in the minimization, and vice versa. The insets show the theoretical values of the transition frequencies calculated by numerically solving the time-independent Schrödinger equation with data taken from [19]. In the maximization experiment these frequencies correspond to transitions of the $^{39}K^{85}Rb$ isotopomer, while in the minimizing experiment the peaks can be assigned to transitions of the $^{41}K^{87}Rb$ isotopomer. By comparing both spectra, a shift between the characteristic peaks is observed. Most importantly, where the spectral intensity is high in the optimal spectrum obtained for maximization, the intensity in the pulse spectrum recorded in the minimization case is very low, and vice versa. This phenomenon was also observed in our previous isotope selective coherent control experiments performed on K_2 and NaK isotopomers [16,17] and is a key factor for achieving high isotope selective ion production.

Besides the peaks associated to transitions from the electronic ground state $X(1)^1\Sigma^+$ to the first excited $A(2)^1\Sigma^+$ state, a few other sharp maxima in the optimized spectra are visible. They contribute most likely to

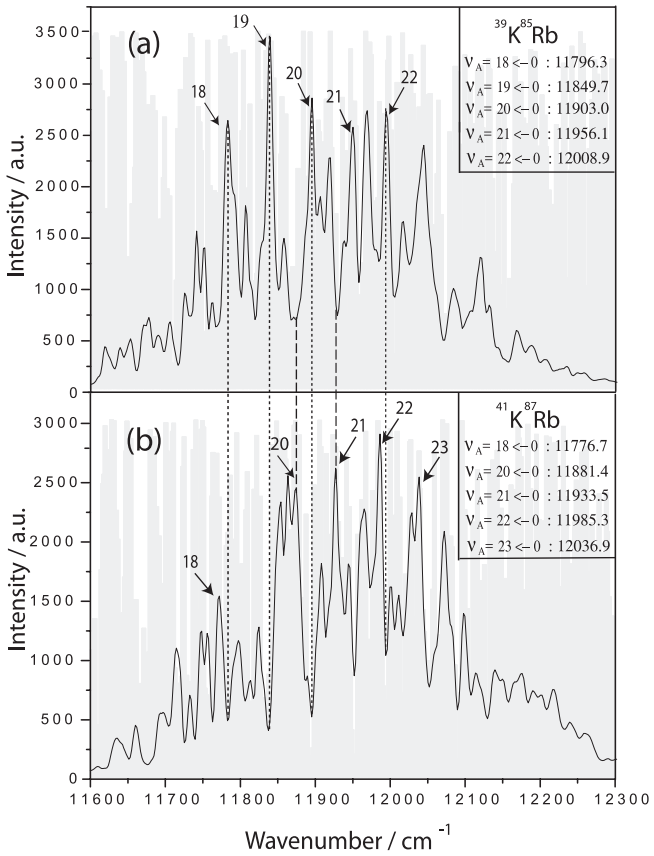

Fig. 1. Optimized pulse spectra obtained for maximization (a) and minimization (b) of the isotopomer ratio $^{39}K^{85}Rb^+/^{41}K^{87}Rb^+$ with simultaneous phase and amplitude modulation. The insets of (a) and (b) show the calculated values of transition frequencies (in cm^{-1}) from $v'' = 0$ of $X(1)^1\Sigma^+$ to the noted vibrational levels of $A(2)^1\Sigma^+$ of the lighter and the heavier isotopomers, respectively. The dashed and dotted lines display the correlation between the dominant peaks: in the maximization experiment the peaks are located at positions where the intensities are low in the minimization case (dotted), and vice versa (dashed). The gray bars represent the corresponding transmission pixel pattern of the optimized pulses. The real resolution of the shaper is reflected by multiplying the pattern with a Gaussian.

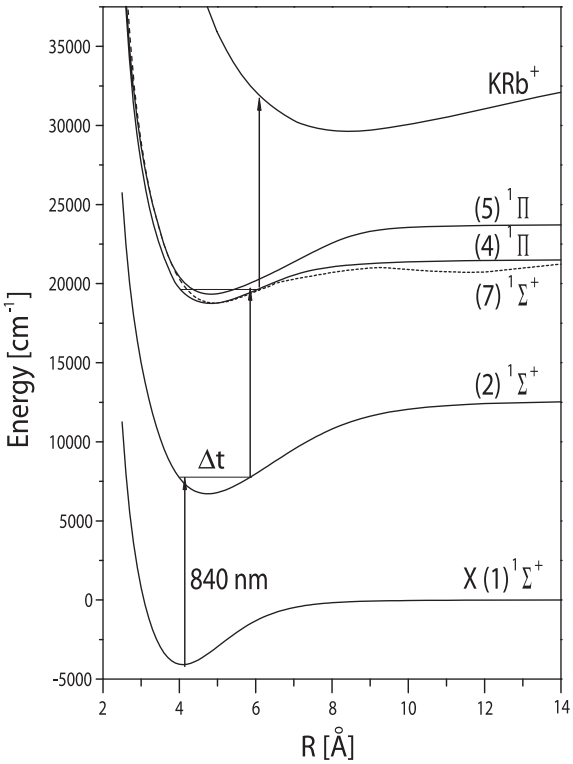

Fig. 2. (a) Calculated potential energy curves [19] of the KRb dimer system. Only those curves are shown which are relevant at the central excitation wavelength of $\lambda = 840$ nm used in the experiment.

transitions into energetically higher located excited states which are also involved in the three photon ionization process. The corresponding scheme is depicted in Figure 2 in which only the experimentally accessible potential energy curves are shown [19]. After the initial excitation step, the system oscillates in the $A(2)^1\Sigma^+$ state with an oscillation period of $\Delta t = 580$ fs. The value of the vibration period was calculated for the $v' = 20$ vibrational level of the first excited state using the spectroscopical constants from [19]. At the favorable location on the $A(2)^1\Sigma^+$ potential energy curve, the wave packet is transferred to the three very close lying excited states $A(7)^1\Sigma^+$, $B(4)^1\Pi$ or $B(5)^1\Pi$. We have to note, that due to the high complexity of the spectra and the fact that the three potentially involved excited states are energetically closely located, an unambiguous identification of the dominant state chosen by the second ionization step is not possible. It should be pointed out that the high resolution allows to selectively address the isotopomer specific vibronic transitions of the first and second excitation step.

In order to complete the optimized pulse characterization and to gain additional details about the isotopomer selective ionization path, intensity cross-correlation and XFROG traces were recorded as well (see Fig. 3). The temporal profile of the optimized laser fields exhibit a large number of clearly distinguishable subpulses in the 30 ps time window. Several multiples of the half-period of the wavepacket oscillation in the $A(2)^1\Sigma^+$ state can often be observed between adjacent subpulses. A detailed explanation of the temporal behavior of the two isotopomers can not be given at this point, also due to the fact that it is not known which state is involved in the second excitation step of the optimized process. The time and frequency shift of the dominant subpulses emerging in the two XFROG traces is indicative of the involvement of different electronic states and the mechanisms during maximization and minimization, respectively. Isotope dependent constructive and destructive interferences of the generated wave packets can also positively contribute to the isotope specific ionization efficiency, as shown by Leibscher and Averbukh [29].

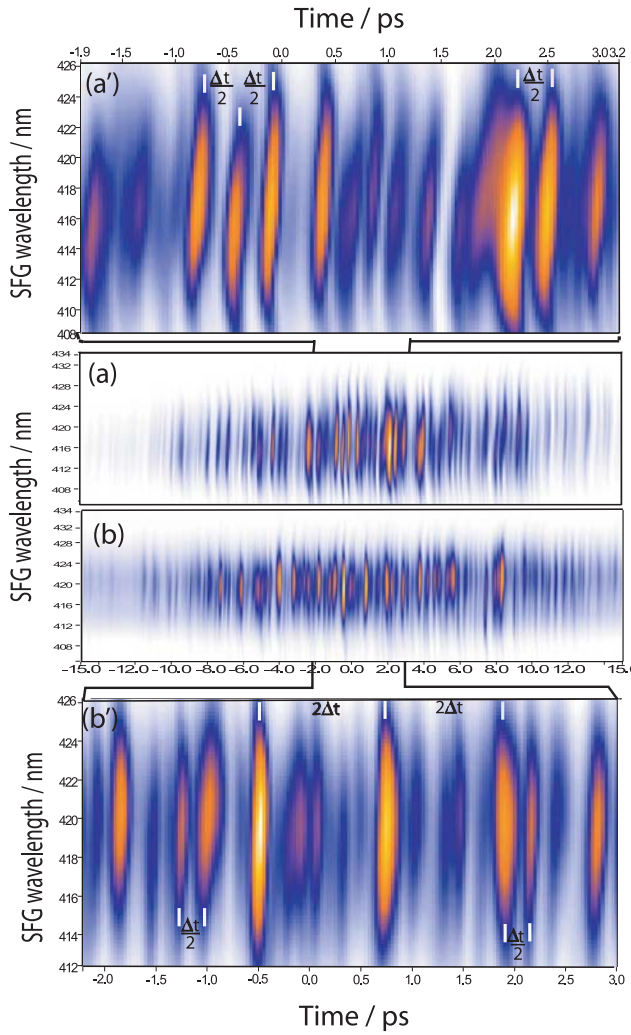

Fig. 3. (Color online) The recorded XFROG traces for phase and amplitude optimization are displayed for maximization (a) and minimization (b) of the isotopomer ratio. (a′) and (b′) show a zoom in the time profile indicating multiples of the half wavepacket oscillation period between the subpulses of the optimized pulse for maximization and minimization, respectively.

4 Conclusion

Isotope selective optimization of the $^{39}K^{85}Rb^+$ and $^{41}K^{87}Rb^+$ ion yields was investigated by applying evolution strategies in a closed loop experiment by using a pulse shaper with the highest commercially available resolution. A factor of about 4 improvement for either maximization or minimization of the $^{39}K^{85}Rb^+$/ $^{41}K^{87}Rb^+$ isotopomer ratio, relative to an unshaped broadband pulse was observed. From the comparison of the optimized pulse spectra with theoretical data, it was possible to clearly identify the vibronic states involved in the initial excitation step. Multiples of wavepacket oscillations in the first excited state were resolved in the recorded XFROG traces. The differences in the time and frequency profile of the pulses indicate different mechanisms and involvement of various excited states in the process of maximization and minimization, respectively.

The authors thank Prof. Gwang-Hi Jeung for the KRb potential energy curves. The Deutsche Forschungsgemeinschaft supported this work in the frame of the Sonderforschungsbereich 450. Andrea Merli acknowledges the Cusanuswerk.

References

1. R.S. Judson, H. Rabitz, Phys. Rev. Lett. **68**, 1500 (1992)
2. I. Rechenberg, *Evolutionsstrategie* (Stuttgart, 1994)
3. C.J. Bardeen, V.V. Yakovlev, K.R. Wilson, A.D. Carpenter, P.M. Weber, W.S. Warren, Chem. Phys. Lett. **280**, 151 (1997)
4. A. Assion, T. Baumert, M. Bergt, T. Brixner, B. Kiefer, V. Seyfried, M. Strehle, G. Gerber, Science **282**, 919 (1998)
5. T.C. Weinacht, J. Ahn, P.H. Bucksbaum, Nature **397**, 233 (1999)
6. A. Glass, T. Rozgonyi, T. Feurer, R. Sauerbrey, G. Szabo, Appl. Phys. B **71**, 1432 (2000)
7. Š. Vajda, A. Bartelt, E.C. Kaposta, T. Leisner, C. Lupulescu, S. Minemoto, P. Rosendo-Francisco, L. Wöste, Chem. Phys. **267**, 231 (2001)
8. T. Brixner, H. Damrauer, G. Gerber, Adv. Mol. Opt. Phys. **46**, 1 (2001)
9. C. Daniel, J. Full, L. Gonzales, C. Lupulescu, J. Manz, A. Merli, Š. Vajda, L. Wöste, Science **299**, 536 (2003)
10. A. Lindinger, C. Lupulescu, F. Vetter, M. Plewicki, S.M. Weber, A. Merli, L. Wöste, J. Chem. Phys. **122**, 024312 (2005)
11. S.A. Rice, Science **258**, 412 (1992)
12. W.S. Warren, H. Rabitz, M. Dahleh, Science **259**, 1581 (1993)
13. K. Sundermann, R. de Vivie de Riedle, App. Phys. B **71**, 285 (2000)
14. H. Rabitz, R. de Vivie-Riedle, M. Motzkus, K. Kompa, Science **288**, 825 (200)
15. B. Schäfer-Bung, R. Mitrić, V. Bonačić-Koutecký, A. Bartelt, C. Lupulescu, A. Lindinger, Š. Vajda, S.M. Weber, L. Wöste, J. Phys. Chem. A **108**, 4175 (2004)
16. A. Lindinger, C. Lupulescu, M. Plewicki, F. Vetter, A. Merli, S. Weber, L. Wöste, Phys. Rev. Lett. **93**, 033001 (2004)
17. A. Lindinger, F. Vetter, C. Lupulescu, M. Plewicki, S. Weber, A. Merli, L. Wöste, Chem. Phys. Lett. **397**, 123 (2004)
18. T. Leininger, G.H. Jeung, Phys. Rev. A **51**, 1929 (1995)
19. S.J. Park, Y.J. Choi, Y.S. Lee, G.H. Jeung, Chem. Phys. **257**, 135 (2000)
20. M.M. Hurley, L.F. Pacios, P.A. Christiansen, R.B. Ross, W.C. Ermler, J. Chem. Phys. **84**, 6840 (1986)
21. Y. Lee, C. Yun, Y. Yoon, T. Kim, B. Kim, J. Chem. Phys. **115**, 7413 (2001)
22. Y. Lee, Y. Yoon, B. Kim, L. Li, S. Lee, J. Chem. Phys. **120**, 6551 (2004)
23. M. Wefers, K. Nelson, J. Opt. Soc. Am. B **12**, 1343 (1995)
24. O.E. Martinez, IEEE J. Quantum Electron. **23**, 59 (1987)
25. A. Monmayrant, B. Chatel, Rev. Sci. Inst. **75**, 2668 (2004)
26. A. Monmayrant, B. Chatel, B. Girard, Opt. Lett. **31**, 410 (2006)
27. A. Monmayrant, B. Chatel, B. Girard, Phys. Rev. Lett. **96**, 103002 (2006)
28. A. Bartels, S. Minemoto, C. Lupulescu, Š. Vajda, L. Wöste, Eur. Phys. J. D **16**, 127 (2001)
29. M. Leibscher, I.S. Averbukh, Phys. Rev. A **63**, 043407 (2001)